Article

Improvement of Distance Protection with SVM on PV-Fed Transmission Lines in Infeed Conditions

Yasar Beyazit Yoldas [1,2,*] and **Recep Yumurtacı** [2]

1 4th Regional Directorate, Turkish Electricity Transmission Corporation, Istanbul 34762, Türkiye
2 Department of Electrical Engineering, Yildiz Technical University, Istanbul 34220, Türkiye
* Correspondence: beyazit.yoldas@std.yildiz.edu.tr

Abstract: Photovoltaic (PV) power plants have comparatively weak infeed characteristics, unlike conventional synchronous generators. The controllability of grid-connected inverters and the limited overcurrent capability of power electronic devices means that the characteristics of faults on transmission lines fed by PV power stations are substantially different than those on transmission lines fed by conventional sources. Operating performances of distance relays on PV-fed transmission line are unveiled. This paper analyses the impact of PV-fed transmission lines in infeed conditions on distance protection. Fault signals on the transmission line were generated by Digsilent PowerFactory software. Then, fault signals were analyzed by discrete Fourier transformation (DFT) with MATLAB software. The measured current and voltage signals were preprocessed first with DFT, and then machine learning via a support vector machine (SVM) was used for regression. This research proposes an improvement on distance protection with SVM for preventing maloperation in infeed conditions on PV fed transmission lines. The average accuracy was up to 95.6% in this study. The simulation was performed at different locations along the transmission line with different types of fault on a given power system model with the PV power plant.

Keywords: distance protection; PV power plant; discrete Fourier transform; support vector machines

1. Introduction

PV power generation has increased in power systems with the rapid development of PV power-generation technology. The integration of a greater number of renewable energy into electric power networks has resulted in a rise in the number of technical challenges for their protection systems.

The fault-current characteristics on the PV power plant side are affected by control approaches, inverter control parameters and power-system fault conditions. The fault current in a transmission line supplied by a PV power plant will have a smaller magnitude than in a transmission line with a conventional power supply [1–3].

The performances of distance relays with Mho characteristics were evaluated in a converter-interfaced microgrid system [4]. It has been shown that the relay operates unnecessarily for the ground faults when a star-connected load is connected downstream of the fault. The performance of distance protection on inverter-interfaced renewable energy generators (IIREGs), including type-IV wind farms (WF) and PV power plants with different control strategies, was analyzed [5]. A novel scheme based on an advanced line-impedance formula is proposed to prevent maloperation on phase–phase–ground faults [6]. The relay's overreach on zone-two faults depends on the IIREG's control strategy. The grid-side boosting current, the measured impedance of the IIREG side, has a large amplitude and phase offset, which causes the conventional distance protection to malfunction or refuse to operate. An improved scheme offered for zero-sequence impedance relay accompanied by a zero sequence over-current starting element constitutes the main protection on the IIREG side [7].

PV power plants have weaker power characteristics during short-circuit faults than traditional power plants of the same capacity [8]. Adaptive distance protection can be used for transmission lines fed with PV power stations. Unlike conventional synchronous generators, the measured impedance varies considerably in magnitude and phase angle [9]. The performance of distance protection against fault components on transmission lines connected to PV power plants was investigated.

Accuracy classification results of three types of artificial intelligence (AI) methods—back-propagation neural networks (BPNN), probabilistic neural networks (PNN) and SVM with wavelet transform (WT)—were compared [10]. A two-phase algorithm consists of discrete wavelet transform (DWT) in the first phase and an SVM in second phase for fault zone identification in a series compensated transmission line [11]. Overall accuracy of 93.917% was reached. The SVM regression method is used for fault location for IEEE 39 bus network [12], for which the input pattern consists of phase voltages and currents. The output pattern is the distance from the substation. A real-time fault detection and classification approach is presented for protective relaying in power transmission systems using SVM with a radial basis function (RBF) kernel [13]. The classification of SVM is based only on the phase angles between the three-phase currents of the transmission line.

A new fault classification approach based on the SVM for a series-compensated transmission line with a fixed-series capacitor located in the middle of the line was presented [14]. The suggested approach uses one-cycle samples of three-line currents and zero-sequence current. The proposed classification method has an accuracy of at least 98%. A methodology utilizing least-square SVM for fault classification and section identification in a series-compensated transmission line was proposed [15]. The proposed scheme uses four binary classifiers: three for selection of three phases and the fourth for ground detection. The average classification rate for all fault types was 97.25%. For an overhead line paired with an underground cable and a 6-bus distribution network, fault classification in power systems was examined using a combination of wavelet transformation and an SVM classifier [16]. Classification accuracy for an overhead line combined with underground cable was between 92.7% and 100%. A DWT combined with multi-resolution analysis (MRA) for fault classification in overhead transmission lines was presented [17]. The technique yields proper results for any type of fault, and it may be used for high fault resistances of up to 500 ohm.

The hyperbolic S-transform was used to extract relevant features from current and voltage signal samples taken from one terminal of a power system [18]. Extracted features were employed for distance protection using support vector classification and support vector regression methods. The effectiveness of the proposed method was investigated by examining various locations of the series capacitor on the transmission line, using a metal oxide varistor to protect the series capacitor from over-voltages.

Power swing, load encroachment, voltage and transient instability, contribute to wrong zone-3 operation. A synchrophasor data-based approach for correct zone-3 operations for distance protection by distinguishing the fault from various stressful scenarios is proposed [19]. The method requires time-synchronized connection and measurement from protection relays.

An SVM-based protection aided communication scheme is presented to reduce distance relay maloperation in unintended distributed generation (DG) tripping circumstances [20]. Average accuracy was between 93.8% and 97.6%. A fault-classification technique for series compensated transmission lines was trained and tested using SVM architecture by producing feature vector using modified full-cycle discrete Fourier transform (MFCDFT) [21]. The suggested algorithm described in this research has been validated for a broad variety of power system scenarios with various degrees of compensation, resulting in a classifier accuracy of 99.5%. Combined DFT and fuzzy-based faulty phase selection and classification in a series compensated transmission line is proposed [22]. Current and voltage phasors are used as inputs for the method. Distance-protection-zone-3 misoperation was also investigated. Various approaches other than machine learning techniques to solve

the problem have been surveyed [23]. Communication-assisted schemes and modifications to local distance protections were examined.

An analysis was conducted of the use of classical machine learning algorithms for protection relay tasks, focusing on nearest neighbors, logistic regression and support vector techniques. The reference support vector machine approach, which achieves error-free categorization of simulated circumstances, is preferred for application [24]. SVM and artificial neural network (ANN)-based approaches for detecting and classifying transmission-line faults in the presence of wind energy sources are used [25]. The SVM classifier outperformed the ANN in terms of classification efficiency and classification time.

The supervision-based blocking strategy was proposed to prevent zone-3 distance relay malfunction during power swing situations [26]. A deep neural network (DNN) was used to analyze the improved discrete wavelet transform (IM-DWT) coefficient for selecting the operating function of distance relay.

An approach that requires the root-mean-square of one cycle three-phase voltage and current measurements during a fault was proposed [27]. These data serve as input for the development of a module for fault isolation and location. This module is intended as a component of the central protection system. It was designed using support vector machine for fault identification and Gaussian regression for fault-location prediction.

The infeed problem on an industrial distance-protection relay is solved by an echo function. The distance-protection relay at the weak side of the infeed reflects the fault signal back for instantaneous tripping. There are also various communication-assisted distance-protection schemes for infeed conditions. The reach setting of time-delayed zone-3 protection should include the infeed effect caused by short-circuit current sources.

The influence of infeed on transmission lines fed by a PV power station on the sensitivity of the reach setting and the resulting tripping performance of a distance protection scheme constitute the main motivation for this work. The trip region considered for distance protection is quadrilateral characteristics on an R-X plane. Since more accurate results are obtained when working with higher-dimensional data, the SVM method is preferred to improve the distance-protection impedance response.

In the current study, different locations along the transmission line with different types of fault were investigated. For each fault location on the adjacent transmission line, the measured current and voltage signals were calculated with DFT. Fault impedances were precalculated by classical distance-protection methods. The fault impedance was estimated using SVM with the suggested technique using currents and voltages in addition to impedance, rather than just using current and voltage data for SVM regression.

2. System Description

The utilization of renewable energy sources such as PV and wind has increased. Large-scale implementation of these energy sources requires effective usage of grid-connected power electronic inverters.

2.1. Overview of the Power System

In this study, an 850 MW PV power plant in Karapinar, Konya, in Turkey, was considered as the sample system. PV units were modeled as one combined unit for ease. Grid-connected PV inverters were realized by employing 0.66/34.5 kV (Dyn11) step-up transformers between the PV system and grid-connected power transformer. The system was connected to the grid through 34.5/400 kV (YNyn0) power transformers. The power system is given in Figure 1. R1 relay is located on the PV-HV busbar side of the L1 line. Transmission line data are shown on Table 1.
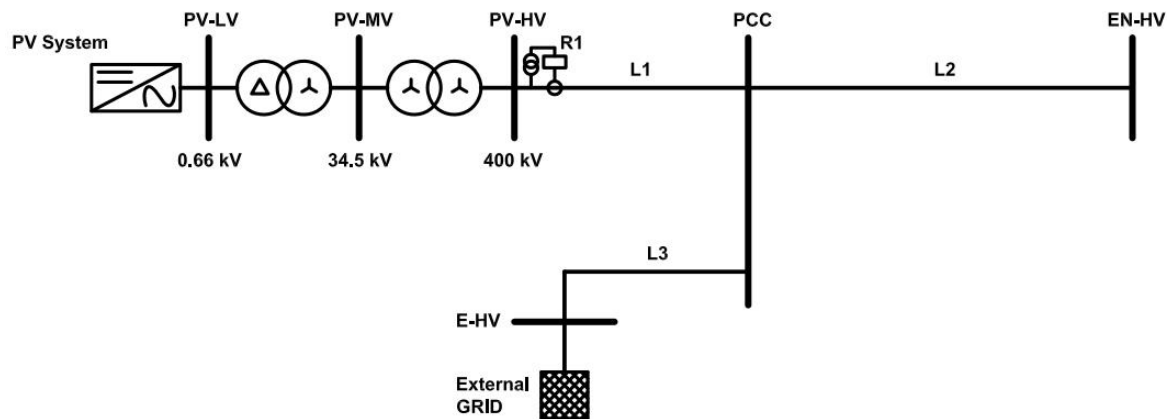
Figure 1. Power system model.

Table 1. Transmission line data.

Line	Length (km)	Conductor Type	Positive Sequence Impedance (Ω)	Zero Sequence Impedance (Ω)
L1	1	ACSR 265/35–380 kV	0.027199 + j0.252555	0.126249 + j0.906360
L2	25	ACSR 265/35–380 kV	0.679996 + j6.313825	3.156225 + j22.6590075
L3	1	ACSR 265/35–380 kV	0.027199 + j0.252555	0.126249 + j0.906360

2.2. PV Power Plant Model

The PV power plant's fault response is determined by the inverter control strategy. The voltage and current values to be measured by the distance-protection relays change with the output response of the inverter.

Transmission-line protection systems utilize negative sequence quantities to determine fault direction distinctly. In case of strictly positive sequence currents, providing negative sequence current in addition to positive sequence current, will help to avoid the occurrence of overvoltages on the unfaulted phases.

There is normally at least one delta/Wye transformer between the inverter terminals, and grounded source transformers are an effective way to supply zero-sequence currents. Hence, inverter-based resources are not required to provide zero-sequence current.

Current-fed inverters are used when the power supply is a physical current source, such as a PV generator. In PowerFactory, the converter is implemented by choosing a static generator element that is configured to function as a current-controlled voltage source converter (VSC).

The control system for a current-controlled VSC model comprises of a slower outer controller and a faster inner current controller. Voltage on the DC side is regulated by the outer controller. Since the DC voltage is assumed to be constant, the outer controller is not used.

The modeling stage is replaced by three ideal voltage sources for simplicity. DC-side dynamics are neglected in Figure 2.

The output power and AC side voltage at the PCC busbar generates current references for the inner current controller, which regulates converter current. The converter currents are controlled using a *d–q* rotating reference system current controller, which regulates the active and reactive current. The active current corresponds to the active power; reactive current corresponds to the reactive power. Both of the currents are regulated by proportional integral (PI) controller.

Phase locked loop (PLL) tracks the inverter voltage with a reference voltage measured at the PCC. It also follows the grid voltage's phase angle.
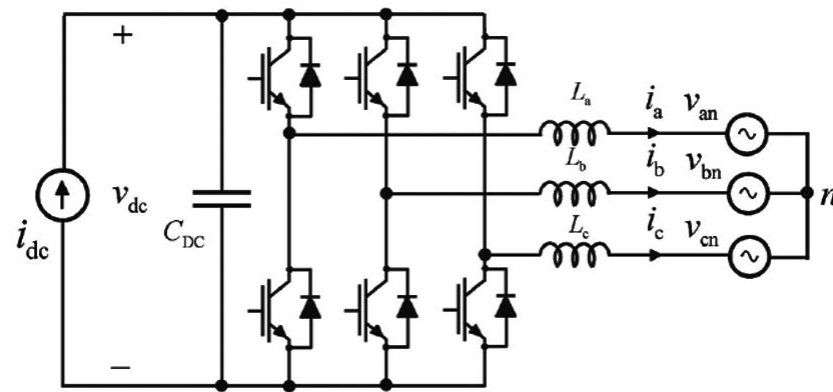
Figure 2. Grid-connected PV system model.

Voltage and current-controlled VSC dynamic models are designed without the effect of load and source impedance. The dynamic models of VSC are derived in the *d–q* domain. where three-phase sinusoidal signals can be analyzed as equivalent DC signals. A detailed PV inverter diagram with controller is shown on Figure 3.
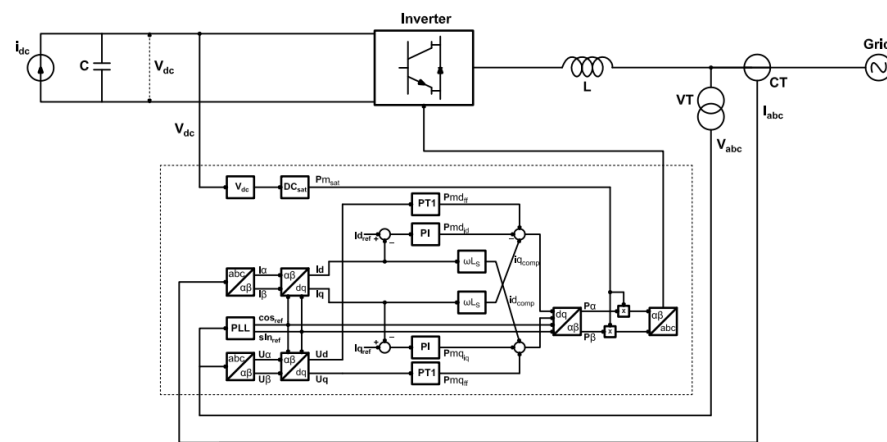

Figure 3. PV-inverter block diagram.

The three-dimensional vectors are converted into two-dimensional rotating vectors with Clarke transformation; the two-dimensional rotating vector is converted to a two-dimensional stationary one with Park transformation.

The command i_{dref} is delivered to a *d–q* frame, a current-control scheme that forces i_d to track i_{dref}. The control of i_d enables the control of P_{md_id}. V_{dc} is limited by a saturation block to protect the VSC against overload and external faults. The current-control scheme also causes i_q = to track i_{qref}. Qs is proportional to i_q.

$$P_{md\_id} = K_d \left(1 + \frac{1}{sT_d}\right) \cdot (i_{dref} - i_d) \tag{1}$$

$$P_{mq\_iq} = K_q \left(1 + \frac{1}{sT_q}\right) \cdot (i_{qref} - i_q) \tag{2}$$

$$P_{md\_ff} = \left(\frac{K_{ff}}{1 + sT_m}\right) \cdot U_d \tag{3}$$

$$P_{mq\_ff} = \left(\frac{K_{ff}}{1 + sT_m}\right) \cdot U_q \tag{4}$$

Based on the VSC safe-operating-current rating, the maximum permitted current magnitude is established and enforced through the application of a saturation limit i_{dref}. The maximum current rating is also a design choice.

2.3. Discrete Fourier Transform

Estimation of the amplitude and phase of the waveform needs to be provided to the relay. A well recognized and the most-used kind of estimation is DFT.

The real and imaginary components of the fundamental frequency phasor are calculated using a sequence of N (number of samples per cycle) uniformly spaced data samples obtained over the whole cycle's data-frame window. As new samples of voltages and currents become available, the window gradually advances by one sample. In order to maintain a constant length of the data window of N samples, the most recent sample is included in the data window, and the oldest sample is discarded.

The Fourier series is based on the assumption that a set of phasors have frequencies that are integer multiples of a fundamental frequency.

$$x(t) = \sum_{k=-N}^{N} A_k \, e^{j(k\omega_0 t)} \tag{5}$$

Replace the continuous function in Equation (5), t, with a function in the discrete domain that progresses in jumps of $\omega_0 T_S$; thus, a phasor of a single frequency would be:

$$x(n) = A \, e^{j(n\omega T_S + \alpha)} \tag{6}$$

$$e^{j(n\omega T_S)} = \cos(n\omega T_S) + j\sin(n\omega T_S) \tag{7}$$

$$x(n) = \sum_{k=-N}^{N} A_k \, e^{j(k\omega_0 T_S n)} \tag{8}$$

T_S is the sampling interval. A_1 is the fundamental frequency phasor value. θ_1 is the phase angle in Equations (9) and (10).

$$A_1 = \sqrt{X_{1real}^2 + X_{1imag}^2} \tag{9}$$

$$\theta_1 = \tan\left(\frac{X_{1imag}}{X_{1real}}\right) \tag{10}$$

2.4. Distance Protection

Distance relays calculate fault impedance using the voltage provided by the voltage transformer (VT) and the current information provided by the current transformer (CT). Table 2 shows calculations used in the measurement of fault impedance for different fault types. Calculated impedance is compared to a predetermined impedance value, and the relay chooses whether to send a trip signal to the circuit breakers based on that.

Table 2. Impedance calculations for different fault types.

Fault Types	Calculation
AG	$V_A / (I_A + 3k_0 I_0)$
BG	$V_B / (I_B + 3k_0 I_0)$
CG	$V_C / (I_C + 3k_0 I_0)$
AB or ABG	$(V_A - V_B)/(I_A - I_B)$
BC or BCG	$(V_B - V_C)/(I_B - I_C)$
CA or CAG	$(V_C - V_A)/(I_C - I_A)$
ABC	V_A / I_A

A, B and C indicate faulty voltage phasors V_A, V_B and V_C; I_A, I_B and I_C are current phasors. Z_0 = line zero-sequence impedance, Z_1 = line positive-sequence impedance, k_0 = residual compensation factor where $k_0 = (Z_0 - Z_1)/3Z_1$.

Faults in the power system could be symmetrical or asymmetrical in nature. All phases of a three-phase fault are in contact with each other, making it a symmetrical fault. Asymmetrical faults are unbalanced faults, including phase–phase (L-L) faults, phase–phase to ground (LL-G) and single phase–ground (SLG) faults. Fault impedance is calculated by using measurements between the faulted phases in case of L-L faults and between faulted phase and neutral in the case of earth faults.

The infeed effect on the measured impedance is a determining factor for distance protection on adjacent lines. In Figure 4, infeed condition occurs in case of faults between BC line, including distance protection zone 2 (Z_2) and zone 3 (Z_3).
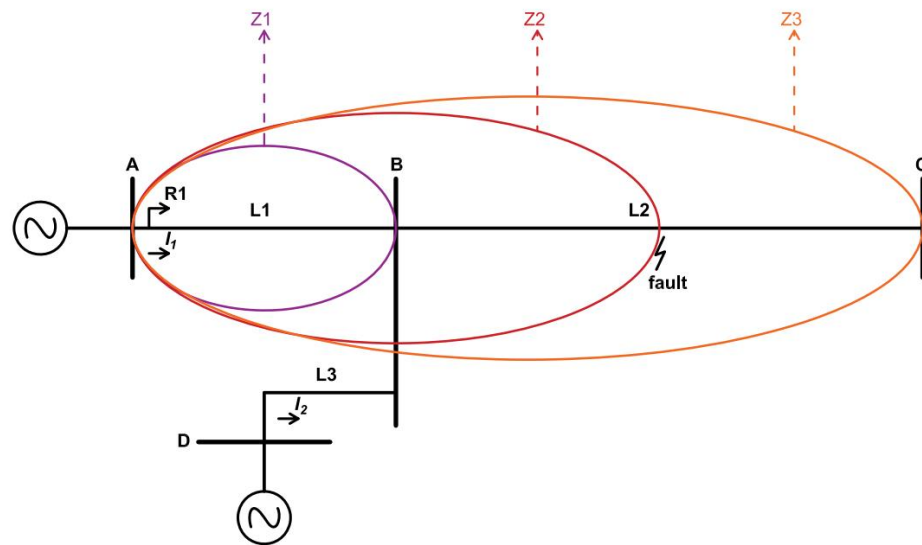

Figure 4. Infeed conditions on the transmission line.

The impedance seen by the R1 distance relay is affected by infeed current. The R1 relay impedance value is shown in Equation (11):

$$Z = Z_1 + \left(\frac{I_1 + I_2}{I_1} \right) Z_2 \tag{11}$$

A distance-protection relay is said to underreach when the impedance seen by the relay due to a fault is greater than the total fault impedance value, even though the fault point is within the protected zone of the line. The relay does not operate correctly. It is called underreach of the relay. Underreach of distance-protection relay is observed due to remote infeed. Remote infeed means the fault is being fed through a different circuit other than the protected line. The remote infeed current is lower than the infeed current for underreaching of distance relay.

If the distance-protection relay reaches beyond its set distance and causes an unselective trip, it is called overreaching of distance relay. The impedance seen by the relay due to a fault is less than the total fault impedance value, even though the actual fault location is out of the protected zone of the line. The remote infeed current is higher than the infeed current for overreaching of distance relay.

2.5. Support Vector Machines

SVM is a machine learning method used mainly for classification and regression-based problems. SVM is a form of supervised learning, which is a type of statistical learning in which a series of examples is used to create a "decision-maker" system that attempts to

predict new values. SVM covers both advanced methods for handling large datasets and the quadratic (or convex) programming part.

We can write the problem as an optimization problem:

$$\min_{w} \frac{1}{2} w^T \cdot w \tag{12}$$

$$subject\ to \begin{cases} y_i - (w^T \cdot \phi(x) + b) \leq \varepsilon \\ (w^T \cdot \phi(x) + b) - y_i \leq \varepsilon \end{cases} \tag{13}$$

$\phi(x)$ is the kernel function, w is the margin, (x_i and y_i) is the training set. We add a bond in order to set the tolerance on the errors number that can be committed for regression:

$$\min_{w,b} \frac{1}{2} w^T \cdot w + C \sum_{i=1}^{l} (\xi_i + \xi_i^*) \tag{14}$$

$$subject\ to \begin{cases} y_i - (w^T \cdot \phi(x) + b) \leq \varepsilon + \xi_i \\ (w^T \cdot \phi(x) + b) - y_i \leq \varepsilon + \xi_i^* \\ \xi_i, \xi_i^* \geq 0, i = 1 \dots l \end{cases} \tag{15}$$

Once trained, SVM regression will generate predictions using the formula:

$$f(x) = \sum_{i=1}^{l} \theta_i\ \phi(x, x_i) + b \tag{16}$$

3. Fault Simulation on System Model

The location of the selected short-circuits on the transmission line between the PCC busbar and the EN-HV busbar. Three different fault scenarios are considered: single-phase ground fault, phase–phase fault and three-phase fault. Inverters operated at a power factor of 0.93 prior to the fault, as planned for operation. A 100 MW load at 1 pf was connected to the PCC busbar for stable pre-fault conditions for a power system.

The control is able to limit the current injection during faults to the nominal but also to an overload current limitation of the generation system. Due to the characteristics of the PV inverter, short-circuit current is equal to 1.2 times the rated current, which is much substantially less than short-circuit current of the synchronous generator at the external grid.

Current is nonetheless limited in magnitude, due to the limit on idref. Current imbalance results in oscillations in the output power of the PV system as well as a decline in its average value. Voltage waveform undergoes notable fluctuations caused by the current-controlled VSC transient response at the beginning of the fault.

Simulations were executed at a system frequency 50 Hz and a sampling frequency of 2 kHz.

The electromagnetic transients (EMT)-type simulation was performed using the Digsilent PowerFactory software. The duration of each pre-fault was 199 ms; the fault was 300 ms. The external grid model uses standard components from the Digsilent PowerFactory library.

We considered the distance-protection relay is connected to L1 line from the PV-HV busbar side. Forward direction is to the PCC busbar. Zones of the distance protection involve zone 1 for the L1 line, zone 2 for the L3 line and zone 3 for the L2 line.

All fault types on the transmission line have been applied at 0% and 95% of the L2 transmission line. Fault resistance is considered zero for all fault types. All measurements and calculations for distance protection are in primary values. L2 line fault location for 0% equals to the total line impedance of the L1 line.

The performance of relay was evaluated by utilizing the practices defined for evaluating the effect of PV power plant remote infeed on distance protection.

Figure 5 illustrates the behavior of the generation units during a single phase–ground fault on phase A at 25% of the L2 line. The fault started at 100 ms. The phase-A pre-fault

voltage peak value was 326 kV. The fault voltage peak decreased to 67 kV. The fault current reached 8.6 kA, becoming stable at a 7.7 kA peak value. An unsymmetrical fault led the zero-sequence voltage on the PV-HV busbar to rise to 29.8 kV, and zero-sequence current increased correspondingly to 2.8 kA in Figure 6.
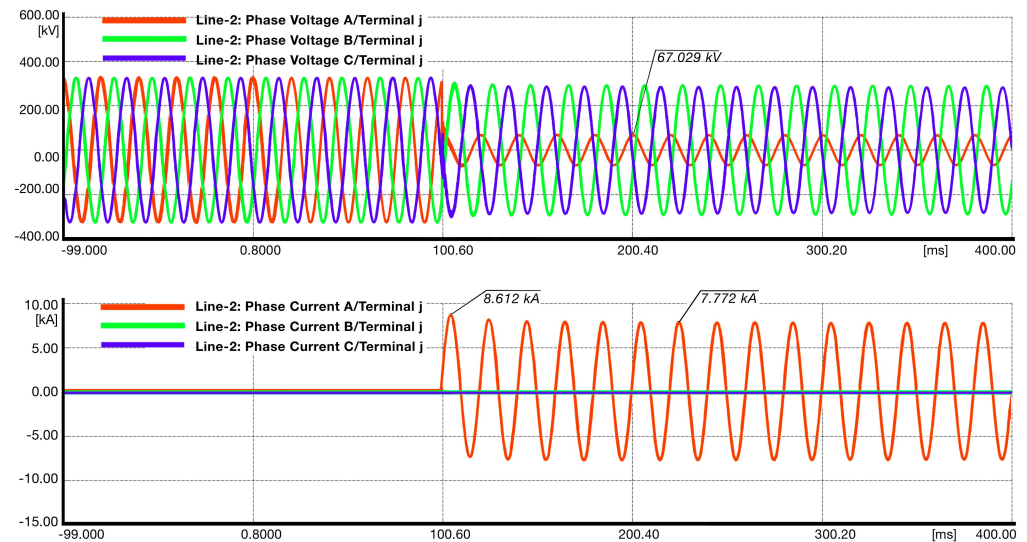

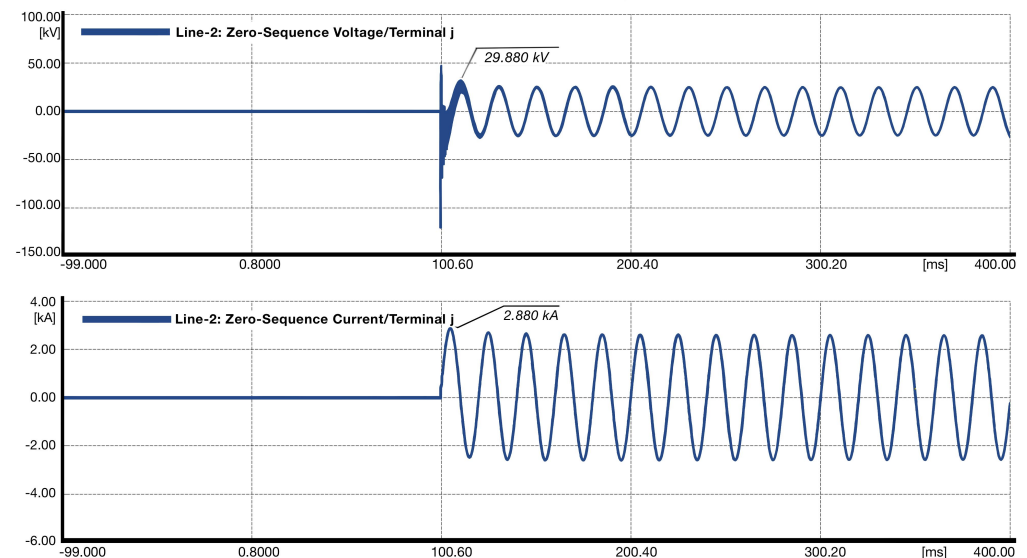**Figure 5.** Three-phase voltages and currents for a single phase–ground fault.

Figure 6. Zero-sequence voltage and current for a single phase–ground fault.

The results of the phase–phase fault at 25% of the L2 line are shown in Figure 7. Peak values went down in faulty phases—for voltage to 160.8 kV and for current to 6.6 kA. Peak fault current stabilized at 5.6 kA. An unsymmetrical fault led to a zero-sequence voltage rise of roughly 12.8 kV, and zero-sequence current was neglected, as seen in Figure 8.

Figure 9 shows a symmetrical three-phase short-circuit fault on the given model. The fault leads to a voltage collapse at the PV-HV busbar, and the peak value of voltage decays to 32.3 kV. The peak value of current reaches 9.2 kA at the beginning of the fault and becomes stable at 6.5 kA. The three-phase fault at the 25% of the L2 line is shown in Figure 10. The zero-sequence voltage peak is 11.6 kV. The zero-sequence currents are low due to the balanced characteristics of three-phase faults.
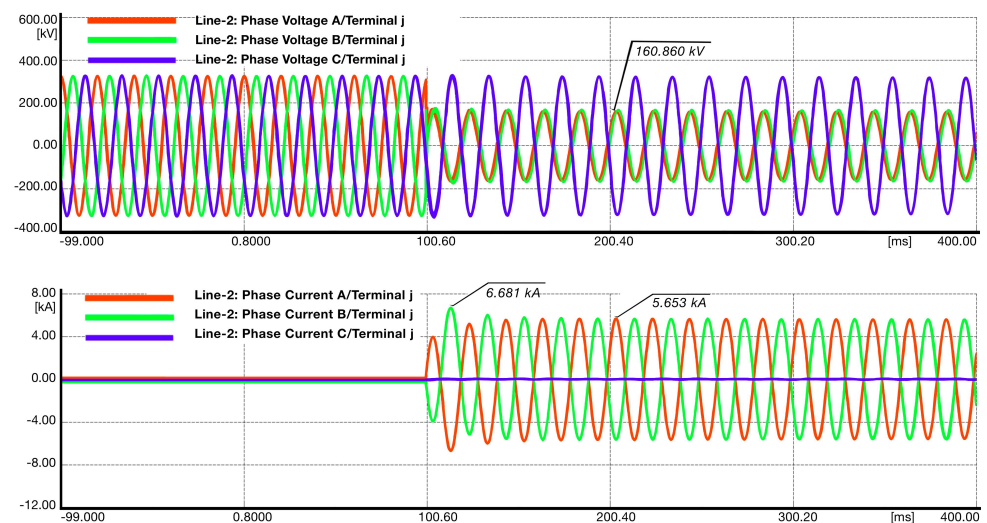
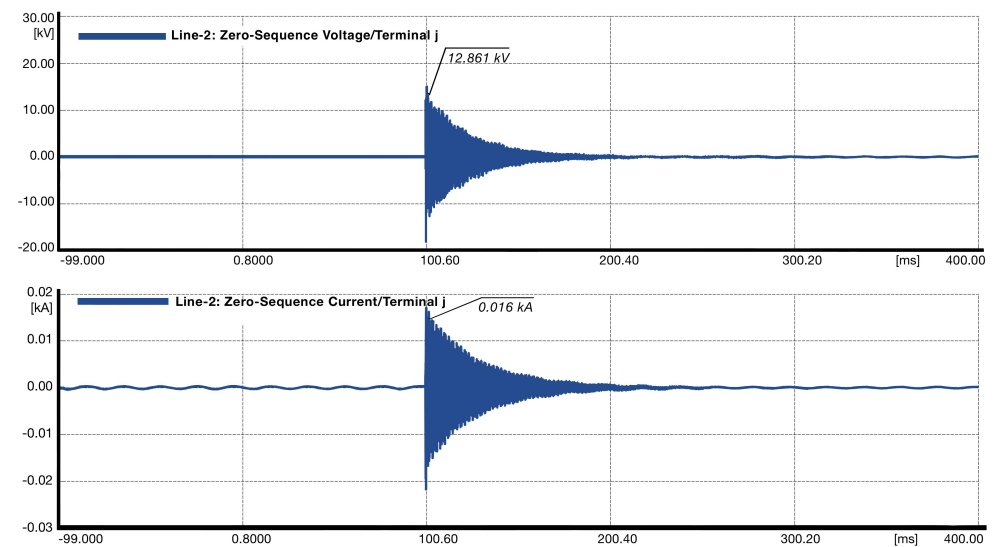**Figure 7.** Three-phase voltages and currents for phase–ground fault.

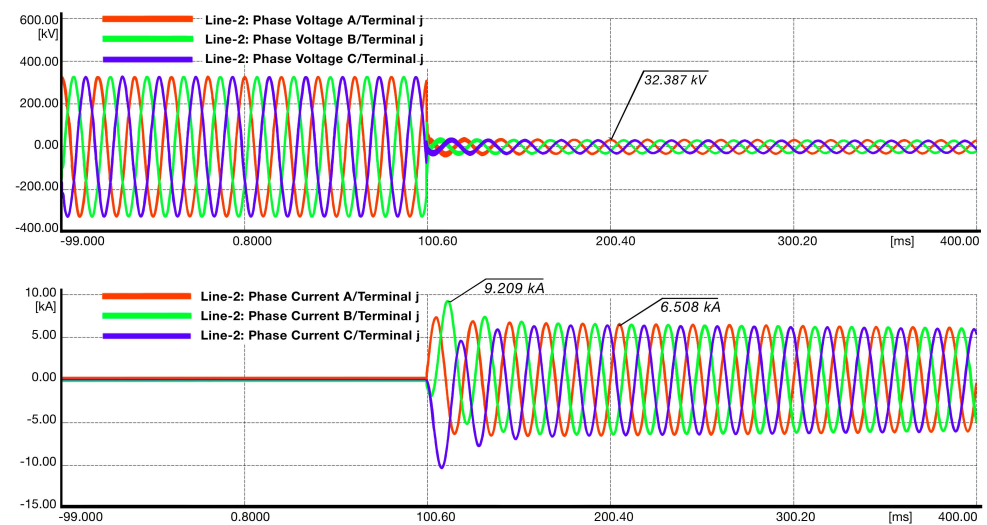**Figure 8.** Zero-sequence voltage and current for phase–ground fault.

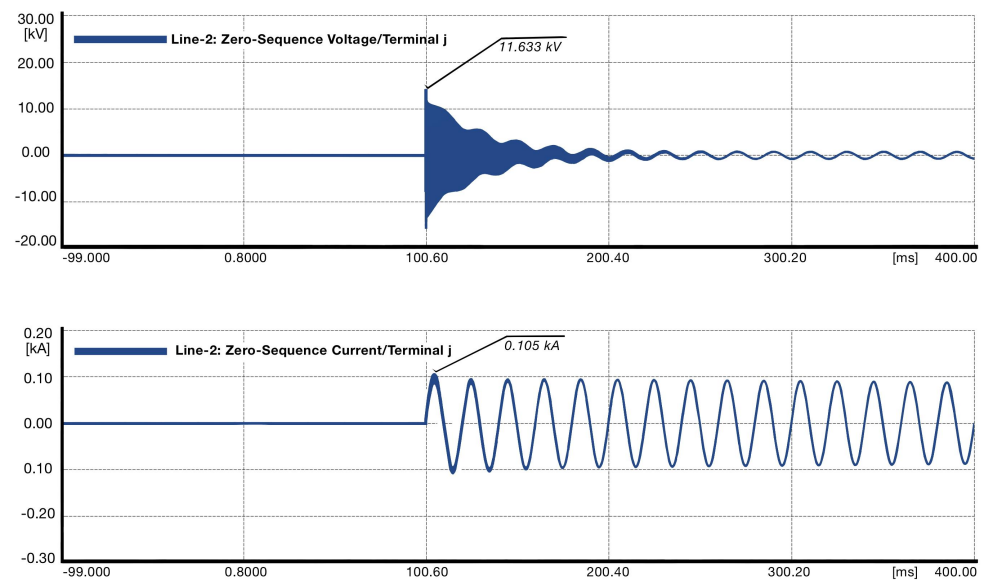**Figure 9.** Three-phase voltages and currents for a three-phase fault.

Figure 10. Zero-sequence voltage and current for a three-phase fault.

4. Evaluation of the Proposed Model

The system load is also represented by a model of constant impedance that contributes nothing to the fault. The fault current peak reached about 9.2 kA in a three-phase fault simulation.

The external grid supports a fault with reactive power. The PV power plant supports a fault with active power. Infeed currents due to PV power plant flow are less than 25% of total fault current.

During phase–ground or phase–ground faults, the underreach or overreach caused by the remote infeed will become very large.

The overall flowchart and diagram of the proposed method are depicted in Figure 11. Current and voltage signals are acquired by short-circuit fault simulation of the power system model. Current and voltage phasors are calculated with DFT. The impedance is a complex value, and its calculation requires the current and voltage phasors or their real and imaginary parts. Phasors are used calculating the impedance values as in distance protection. Current, voltage and impedance values are combined in fault-type classified datasets. In SVM regression, datasets are used as an input for quadratic kernel method.

L2 line impedance is the actual impedance of the L2 line. Fault impedance with DFT is impedance calculated with the use of DFT method with measured voltage and current values. Total fault impedance value shows the sum of the L1 line and L2 line impedance, which is the expected impedance value from the distance-protection relay. Impedance values are calculated in the proposed model as fault impedance with a SVM.

Simulation results indicate that the fault impedance measured with DFT is significantly affected by fault type in various fault locations (0–95%) of the L2 line. Fault impedance with SVM, which clearly shows the efficacy of the proposed method, clearly distinguishes the faults for different sections of transmission line. Error decreased in the course of training the model for all fault types.

Measured fault impedance is much less than the total fault impedance. Distance relay underreached and performs more successfully for phase–ground faults, as seen in DFT values. In Figure 12, impedance with DFT values change linearly due to fault location. Measured and calculated impedance values are shown in Table 3.

Fault impedance with the SVM method values reached normal values of total fault impedance, as expected. Error decreased with steps of the learning algorithm. The average accuracy for phase–ground faults was 92.1%.
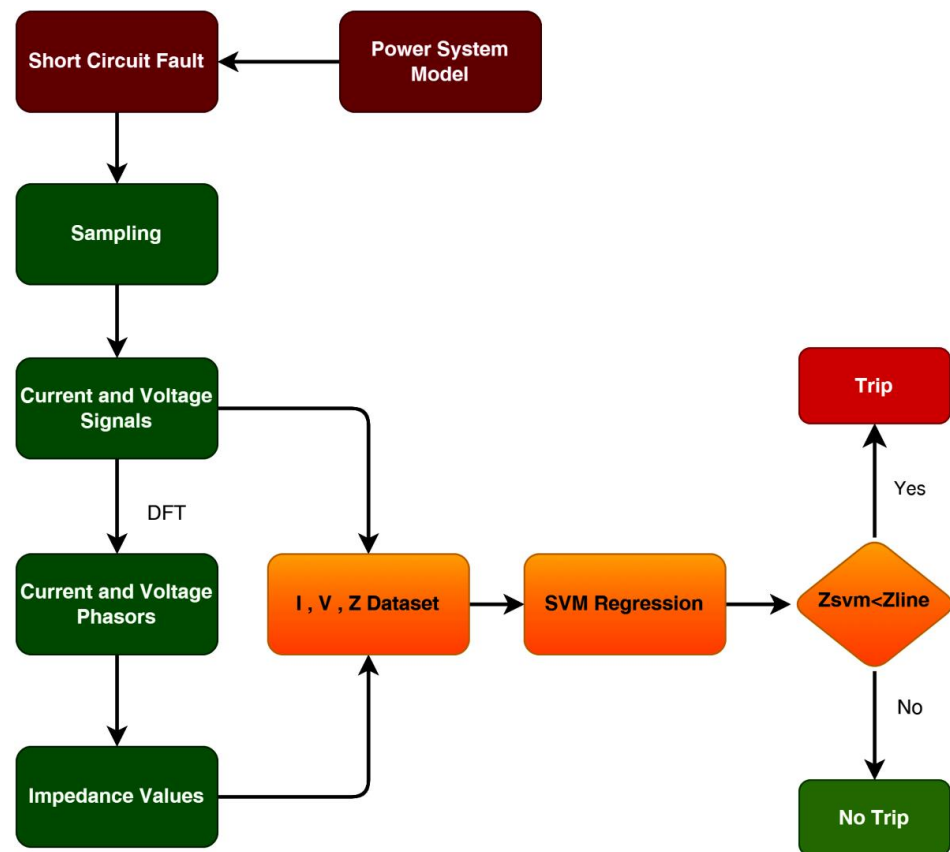
Figure 11. Proposed distance protection with the SVM method.

Table 3. Impedance-fault locations for single phase–ground faults.

L2 Line Fault Location (%)	L2 Line imp. (Ω)	Fault imp. with DFT (Ω)	Total Fault imp. (Ω)	Fault imp. with SVM (Ω)	Error (%)
0	0	0.0027	0.2540	0.3490	37.3784
5	0.3157	0.2598	0.5715	0.6798	18.9357
10	0.6314	0.5195	0.8890	1.1041	24.1944
15	0.9471	0.7792	1.2066	1.4268	18.2560
20	1.2628	1.0389	1.5241	1.7117	12.3135
25	1.5785	1.2985	1.8416	2.0043	8.8323
30	1.8942	1.5581	2.1591	2.3032	6.6731
35	2.2099	1.8178	2.4766	2.6151	5.5898
40	2.5256	2.0773	2.7941	2.9511	5.6157
45	2.8413	2.3369	3.1117	3.2157	3.3448
50	3.157	2.5974	3.4292	3.5906	4.7084
55	3.4727	2.8559	3.7467	3.6640	2.2060
60	3.7884	3.1147	4.0642	4.1621	2.4094
65	4.1041	3.3747	4.3817	4.4824	2.2975
70	4.4198	3.6343	4.6992	4.5705	2.7392
75	4.7355	3.8939	5.0168	4.9431	1.4680
80	5.0512	4.1533	5.3343	5.2740	1.1310
85	5.3669	4.4127	5.6518	5.6021	0.8800
90	5.6826	4.6721	5.9693	5.9407	0.4790
95	5.9983	4.9314	6.2868	6.2881	0.0196

Measured fault impedance at the relay was much larger than the total fault impedance. Phase–phase faults caused the relay to overreach. The DespitPhase distance element with DFT due to remote infeed will not yield successful results if a PV power plant is connected to the line. Nonlinearity of the impedance change can be seen in Figure 13. The deviation

in fault impedance with DFT of the distance-protection relay increases if the fault location is further from the infeed point, as seen in Table 4.
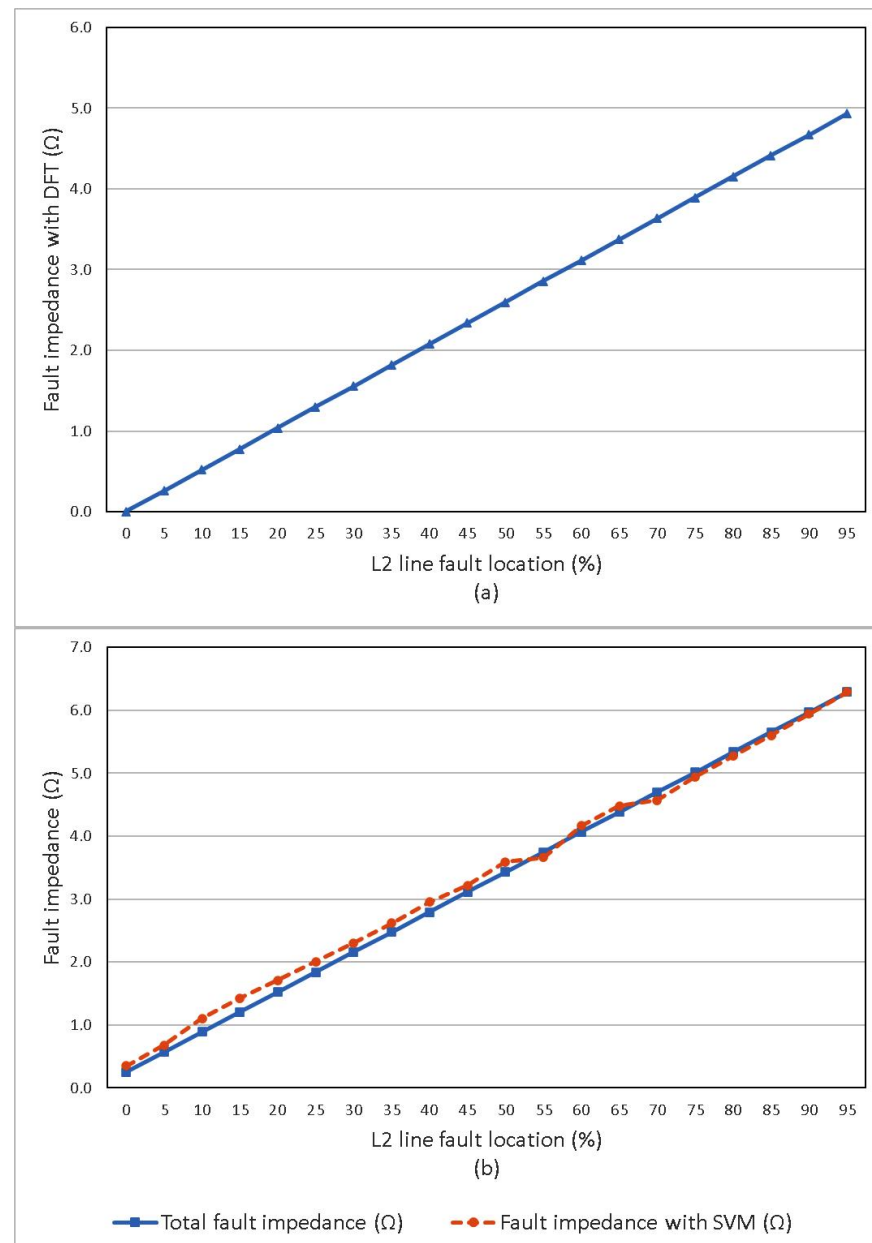

Figure 12. Single phase–ground faults. (**a**) Fault impedance with DFT-fault location. (**b**) Total fault impedance and fault impedance with SVM-fault location.

Fault impedance with the SVM method values reached the normal values of total fault impedance, as expected, which clearly shows the efficacy of the proposed method. The average accuracy for phase–ground faults was 92.2%.

Fault impedance with DFT reached near actual total fault impedance values for three-phase faults. The impedance change seems to have been slightly nonlinear, as seen in Figure 14. Due to the lack of zero-sequence current, the PV power plant had a less negative effect on the three-phase faults. The similarity of fault impedance with DFT and total fault impedance values is shown in Table 5.

Protection performance increased significantly with the SVM method for three-phase short-circuit faults. The average accuracy ascended to 95.6% for three-phase faults.
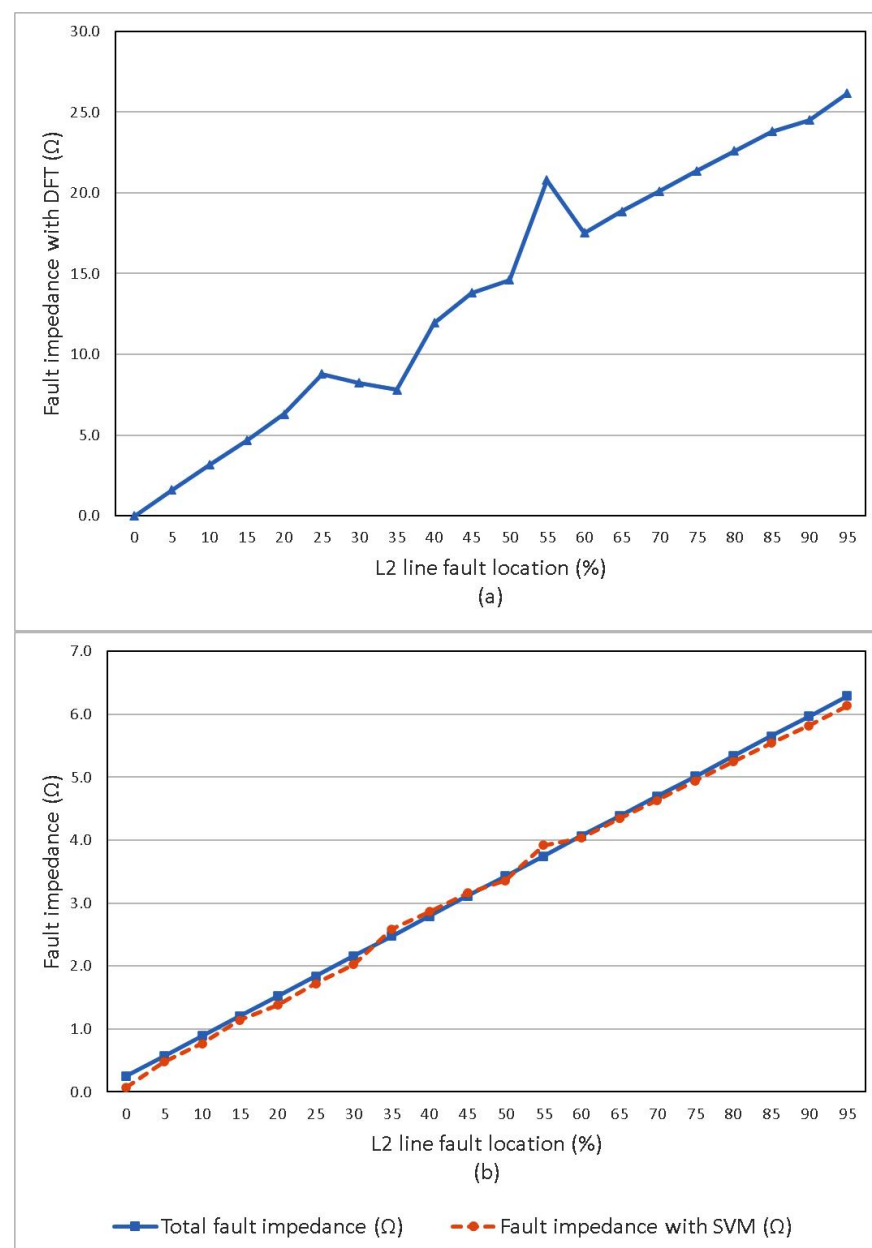
Figure 13. Phase–phase faults. (**a**) Fault impedance with DFT-fault location. (**b**) Total fault impedance and fault impedance with SVM-fault location.

Table 4. Impedance-fault locations for phase–ground faults.

L2 Line Fault Location (%)	L2 Line imp. (Ω)	Fault imp. with DFT (Ω)	Total Fault imp. (Ω)	Fault imp. with SVM (Ω)	Error (%)
0	0	0.0012	0.2540	0.0713	71.9167
5	0.3157	1.5974	0.5715	0.4794	16.1151
10	0.6314	3.1547	0.8890	0.7709	13.2886
15	0.9471	4.6746	1.2066	1.1436	5.2183
20	1.2628	6.2892	1.5241	1.3839	9.1951
25	1.5785	8.7853	1.8416	1.7226	6.4638
30	1.8942	8.2242	2.1591	2.0268	6.1299
35	2.2099	7.8073	2.4766	2.5860	4.4175
40	2.5256	11.9504	2.7941	2.8653	2.5453
45	2.8413	13.7992	3.1117	3.1618	1.6106

Table 4. *Cont.*

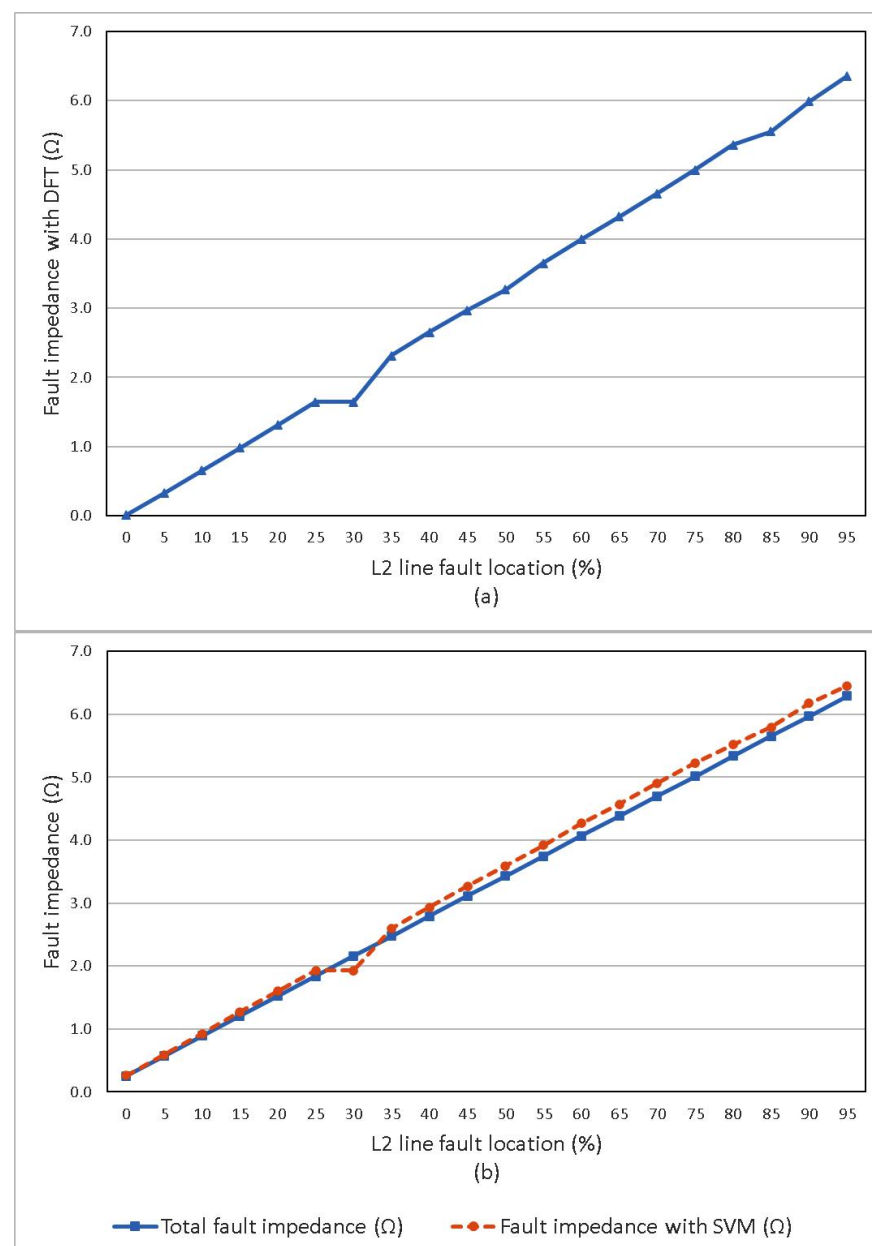| L2 Line Fault Location (%)	L2 Line imp. (Ω)	Fault imp. with DFT (Ω)	Total Fault imp. (Ω)	Fault imp. with SVM (Ω)	Error (%)
50	3.157	14.6038	3.4292	3.3607	1.9978
55	3.4727	20.7931	3.7467	3.9177	4.5630
60	3.7884	17.5354	4.0642	4.0382	0.6396
65	4.1041	18.8662	4.3817	4.3444	0.8519
70	4.4198	20.1189	4.6992	4.6367	1.3300
75	4.7355	21.3733	5.0168	4.9437	1.4558
80	5.0512	22.5914	5.3343	5.2492	1.5951
85	5.3669	23.7933	5.6518	5.5455	1.8814
90	5.6826	24.5139	5.9693	5.8180	2.5349
95	5.9983	26.1534	6.2868	6.1380	2.3678

Figure 14. Three-phase faults. (**a**) Fault impedance with DFT-fault location. (**b**) Total fault impedance and fault impedance with SVM-fault location.

Table 5. Impedance-fault locations for three-phase faults.

L2 Line Fault Location (%)	L2 Line imp. (Ω)	Fault imp. with DFT (Ω)	Total Fault imp. (Ω)	Fault imp. with SVM (Ω)	Error (%)
0	0	0.0081	0.2540	0.2579	1.5324
5	0.3157	0.3251	0.5715	0.5871	2.7262
10	0.6314	0.6529	0.8890	0.9269	4.2522
15	0.9471	0.9822	1.2066	1.2692	5.1880
20	1.2628	1.3135	1.5241	1.5994	4.9431
25	1.5785	1.6455	1.8416	1.9290	4.7465
30	1.8942	1.6455	2.1591	1.9290	10.6574
35	2.2099	2.3127	2.4766	2.6014	5.0373
40	2.5256	2.6509	2.7941	2.9364	5.0926
45	2.8413	2.9681	3.1117	3.2707	5.1121
50	3.157	3.2707	3.4292	3.5896	4.6766
55	3.4727	3.6508	3.7467	3.9211	4.6543
60	3.7884	3.9929	4.0642	4.2647	4.9341
65	4.1041	4.3215	4.3817	4.5687	4.2667
70	4.4198	4.6578	4.6992	4.9079	4.4406
75	4.7355	4.9997	5.0168	5.2257	4.1654
80	5.0512	5.3587	5.3343	5.5168	3.4210
85	5.3669	5.5544	5.6518	5.7932	2.5018
90	5.6826	5.9883	5.9693	6.1728	3.4096
95	5.9983	6.3483	6.2868	6.4490	2.5789

5. Conclusions

Three different fault types for addressing the maloperation of distance relays in power systems caused by the infeed effect of PV power plants were presented. It was shown that classical impedance calculation with DFT phasors underreaches for phase–ground faults, overreaches for phase–ground faults with infeed conditions. Distance relay will also fail to detect line faults in zones 2 and 3.

Measured current and voltage signals from the power system model with a PV power plant are preprocessed with DFT; then, the fundamental component magnitudes of three-phase current and voltage signals are used to calculate impedance. These current, voltage and impedance values are applied to the SVM algorithm. Fault impedance is recalculated with the proposed method with SVM for faults on an adjacent transmission line that is also fed by the PV power plant.

In order to estimate line fault-impedance parameters, a particular application of the SVM method was implemented, which operates on measured and calculated samples from the model.

Performance of the proposed distance protection method with machine learning for faults on transmission systems with PV power plant connected to the power system was studied. The results indicate that the proposed distance protection impedance calculation method using a SVM is highly effective and reliable at providing a protection measure for the transmission system with PV power plant integration. Distance-protection relay with the proposed method can operate correctly with different fault types and fault positions. The results obtained showed accuracy of 92.1% to 95.6% for different fault types. The methodology yields quite exact and accurate results.

Different fault resistances can also be studied for future work. Adaptive distance protection can be applied with the investigated method on adjacent transmission lines fed with a PV power plant for further studies.

Data Availability Statement: Not applicable.

Conflicts of Interest: The authors declare no conflict of interest.

Abbreviations

The following abbreviations are used in this manuscript:

AI	Artificial intelligence
ANN	Artificial neural network
BPNN	Back-propagation neural networks
CT	Current transformer
DFT	Discrete Fourier transformation
DG	Distributed generation
DNN	Deep neural network
DWT	Discrete wavelet transform
EMT	Electromagnetic transients
IIREGs	Inverter-interfaced renewable energy generators
IM-DWT	Improved discrete wavelet transform
L-L	Phase-phase
LL-G	Phase-phase to ground
MRA	Multi resolution analysis
MFCDFT	Modified full cycle discrete Fourier transform
PI	Proportional integral
PLL	Phase locked loop
PNN	Probabilistic neural networks
PV	Photovoltaic
RBF	Radial basis function
SLG	Single phase–ground
SVM	Support vector machine
VSC	Voltage source converter
VT	Voltage transformer
WF	Wind farms
WT	Wavelet transform

References

1. Song, H.S.; Nam, K. Dual current control scheme for PWM converter under unbalanced input voltage conditions. *IEEE Trans. Ind. Electron.* **1999**, *46*, 953–959. [CrossRef]
2. Baran, M.E.; El-Markaby, I. Fault Analysis on Distribution Feeders With Distributed Generators. *IEEE Trans. Power Syst.* **2005**, *20*, 1757–1764. [CrossRef]
3. Dewadasa, J.M.; Ghosh, A.; Ledwich, G. Distance Protection Solution for a Converter Controlled Microgrid. In Proceedings of the Fifteenth National Power Systems Conference (NPSC), Bombay, India, 16–18 December 2008.
4. Dewadasa, M.; Ghosh, A.; Ledwich, G. Line Protection in Inverter Supplied Networks. In Proceedings of the 2008 Australasian Universities Power Engineering Conference, Sydney, Australia, 14–17 December 2008.
5. Hooshyar, A.; Azzouz, M.A.; El-Saadany, E.F. Distance Protection of Lines Emanating From Full-Scale Converter-Interfaced Renewable Energy Power Plants-Part I: Problem Statement. *IEEE Trans. Power Deliv.* **2015**, *30*, 1770–1780. [CrossRef]
6. Hooshyar, A.; Azzouz, M.A.; El-Saadany, E.F. Distance Protection of Lines Emanating From Full-Scale Converter-Interfaced Renewable Energy Power Plants-Part II: Solution Description and Evaluation. *IEEE Trans. Power Deliv.* **2015**, *30*, 1781–1791. [CrossRef]
7. Fang, Y.; Jia, K.; Yang, Z.; Li, Y.; Bi, T. Impact of Inverter-Interfaced Renewable Energy Generators on Distance Protection and an Improved Scheme. *IEEE Trans. Ind. Electron.* **2019**, *66*, 7078–7088. [CrossRef]
8. Sun, M.; Wang, H.; Zhu, X. Fault Characteristics of Photovoltaic Power Station and Its Influence on Relay Protection of Transmission Line. In Proceedings of the 5th IET International Conference on Renewable Power Generation (RPG) 2016, London, UK, 21–23 September 2016.
9. Liang, Y.; Xu, G.; Zha, W.; Wang, C. Adaptability Analysis of Fault Component Distance Protection on Transmission Lines Connected to Photovoltaic Power Stations. *Energies* **2019**, *12*, 1578. [CrossRef]
10. Klomjit, J.; Ngaopitakkul, A. Comparison of Artificial Intelligence Methods for Fault Classification of the 115-kV Hybrid Transmission System. *Appl. Sci.* **2020**, *10*, 3967. [CrossRef]
11. Parikh, U.B.; Das, B.; Maheshwari, R.P.P. Combined Wavelet-SVM Technique for Fault Zone Detection in a Series Compensated Transmission Line. *IEEE Trans. Power Deliv.* **2008**, *23*, 1789–1794. [CrossRef]

12. Ravikumar, B.; Thukaram, D.; Khincha, H.P. Application of support vector machines for fault diagnosis in power transmission system. *IET Gener. Transm. Distrib.* **2008**, *2*, 119. [CrossRef]

13. Youssef, O.A.S. An optimised fault classification technique based on Support-Vector-Machines. In Proceedings of the 2009 IEEE/PES Power Systems Conference and Exposition, Seattle, WA, USA, 15–18 March 2009; pp. 1–8.

14. Parikh, U.B.; Das, B.; Maheshwari, R. Fault classification technique for series compensated transmission line using support vector machine. *Int. J. Electr. Power Energy Syst.* **2010**, *32*, 629–636. [CrossRef]

15. Dubey, H.C.; Tiwari, A.K.; Ray, P.K.; Mohanty, S.R.; Kishor, N. A novel fault classification scheme based on least square SVM. In Proceedings of the 2012 Students Conference on Engineering and Systems, Allahabad, India, 16–18 March 2012; pp. 1–5.

16. Livani, H.; Evrenosoglu, C.Y. A fault classification method in power systems using DWT and SVM classifier. In Proceedings of the PES T&D 2012, Orlando, FL, USA, 7–10 May 2012; pp. 1–5.

17. Prasad, A.; Edward, J.B. Application of Wavelet Technique for Fault Classification in Transmission Systems. *Procedia Comput. Sci.* **2016**, *92*, 78–83. [CrossRef]

18. Moravej, Z.; Khederzadeh, M.; Pazoki, M. New Combined Method for Fault Detection, Classification, and Location in Series-compensated Transmission Line. *Electr. Power Components Syst.* **2012**, *40*, 1050–1071. [CrossRef]

19. Kundu, P.; Pradhan, A.K. Synchrophasor-Assisted Zone 3 Operation. *IEEE Trans. Power Deliv.* **2014**, *29*, 660–667. [CrossRef]

20. Legha, M.M.; Mojazi, B.; Mohammadi, M. Preventing Transmission Distance Relays Maloperation under Unintended Dg Tripping Using Svm. *IIOAB J.* **2016**, *7*, 346–355.

21. Patel, U.J.; Chothani, N.G.; Bhatt, P.J. Sequence-space-aided SVM classifier for disturbance detection in series compensated transmission line. *Meas. Technol.* **2018**, *12*, 983–993. [CrossRef]

22. Mishra, P.K.; Yadav, A. Combined DFT and Fuzzy Based Faulty Phase Selection and Classification in a Series Compensated Transmission Line. *Model. Simul. Eng.* **2019**, *2019*, 1–18. [CrossRef]

23. Abdullah, A.M.; Butler-Purry, K. Distance protection zone 3 misoperation during system wide cascading events: The problem and a survey of solutions. *Electr. Power Syst. Res.* **2018**, *154*, 151–159. [CrossRef]

24. Kulikov, A.; Loskutov, A.; Bezdushniy, D. Relay Protection and Automation Algorithms of Electrical Networks Based on Simulation and Machine Learning Methods. *Energies* **2022**, *15*, 6525. [CrossRef]

25. Shah, H.; Chothani, N.; Chakravorty, J. Fault Detection and Classification in Interconnected System with Wind Generation Using ANN and SVM. *AEEE* **2022**, *20*, 225–239. [CrossRef]

26. Sriram, C.; Somlal, J. IM-DWT with DNN Based Blocking Scheme of Third Zone Distance Relay in Power Swing Condition. *Smart Sci.* **2022**, 1–20. [CrossRef]

27. Srivastava, A.; Parida, S.K. A Robust Fault Detection and Location Prediction Module Using Support Vector Machine and Gaussian Process Regression for AC Microgrid. *IEEE Trans. Ind. Appl.* **2022**, *58*, 930–939. [CrossRef]